Wave dynamics on toroidal surface

Wang, Dongyang; Liu, Changxu; Liu, Hongchao; Han, Jiaguang; Zhang, Shuang

DOI:
10.1364/OE.26.017820

Document Version
Publisher's PDF, also known as Version of record

Citation for published version (Harvard):
Wang, D, Liu, C, Liu, H, Han, J & Zhang, S 2018, 'Wave dynamics on toroidal surface', *Optics Express*, vol. 26, no. 14, pp. 17820-17829. https://doi.org/10.1364/OE.26.017820

Research Article | Vol. 26, No. 14 | 9 Jul 2018 | OPTICS EXPRESS 17820
Optics EXPRESS

Wave dynamics on toroidal surface

DONGYANG WANG,[1,2] CHANGXU LIU,[1] HONGCHAO LIU,[1] JIAGUANG HAN,[2] AND SHUANG ZHANG[1,3]

[1]*School of Physics & Astronomy, University of Birmingham, Birmingham, B15 2TT, UK*
[2]*Center for Terahertz Waves and College of Precision Instrument and Optoelectronics Engineering, Tianjin University and the Key Laboratory of Optoelectronics Information and Technology (Ministry of Education), Tianjin 300072, China*
[3]*s.zhang@bham.ac.uk*

Abstract: Wave dynamics on curved surfaces has attracted growing attention due to its close resemblance to the warped space time governed by general relativity. It also opens up opportunities for designing functional optical devices such as geodesic lenses. In this work we study the wave dynamics on the surface of a torus, a shape of considerable interest due to its nontrivial topology. Governed by the conservation of angular momentum, light propagates on the torus in two different types of modes: one is able to twist around and sweep through the whole surface of the torus; the other is confined within a certain angular range along the torus latitude direction. The confined mode exhibits an interesting self focusing or imaging behavior, which, similar to a geometric lens, shows no dependence of wavelength and thus suffers no chromatic aberration. By changing the geometric parameters of the torus, both the focusing point and the focusing distance can be controlled. Our work provides a new approach to manipulation of light propagation on a curved surface under the conservation of angular momentum.

OCIS codes: (240.0240) Optics at surfaces; (240.6648) Surface dynamics; (110.0110) Imaging systems.

References and links

1. A. J. Kox, M. J. Klein, and R. Schulmann, *The Collected Papers of Albert Einstein,* Vol. 6 (Princeton University, 1997).
2. S. W. Hawking, "Black hole explosions?" Nature **248**(5443), 30–31 (1974).
3. W. G. Unruh, "Notes on black-hole evaporation," Phys. Rev. D Part. Fields **14**(4), 870–892 (1976).
4. R. Brout, S. Massar, R. Parentani, and P. Spindel, "A primer for black hold quantum mechanics," Phys. Rep. **260**(6), 329–446 (1995).
5. U. Lenohardt and P. Piwnicki, "Optics of nonuniformly moving media," Phys. Rev. A **60**(6), 4301–4312 (1999).
6. W. G. Unruh, "Experimental Black-Hole Evaporation?" Phys. Rev. Lett. **46**(21), 1351–1353 (1981).
7. C. Barcelo, S. Liberati, and M. Visser, "Probing semiclassical analog gravity in Bose-Einstein condensates with widely tunable interactions," Phys. Rev. A **68**(5), 053613 (2003).
8. T. G. Philbin, C. Kuklewicz, S. Robertson, S. Hill, F. König, and U. Leonhardt, "Fiber-Optical Analog of the Event Horizon," Science **319**(5868), 1367–1370 (2008).
9. R. C. T. da Costa, "Quantum mechanics of a constrained particle," Phys. Rev. A **23**(4), 1982–1987 (1981).
10. U. Leonhardt and P. Piwnicki, "Relativistic Effects of Light in Moving Media with Extremely Low Group Velocity," Phys. Rev. Lett. **84**(5), 822–825 (2000).
11. E. E. Narimanov and A. V. Kildishev, "Optical black hole: Broadband omnidiectional light absorber," Appl. Phys. Lett. **95**(4), 041106 (2009).
12. I. I. Smolyaninov, "Surface Plasmon toy model of a rotating black hole," New J. Phys. **5**, 147 (2003).
13. D. A. Genov, S. Zhang, and X. Zhang, "Mimicking celestial mechanics in metamaterials," Nat. Phys. **5**(9), 687–692 (2009).
14. U. Leonhardt and T. G. Philbin, "General relativity in electrical engineering," New J. Phys. **8**(10), 247 (2006).
15. V. H. Schultheiss, S. Batz, A. Szameit, F. Dreisow, S. Nolte, A. Tünnermann, S. Longhi, and U. Peschel, "Optics in Curved Space," Phys. Rev. Lett. **105**(14), 143901 (2010).
16. C. W. Misner, K. S. Thorne, and J. A. Wheeler, *Gravitation* (W. H. Freeman, 1973).
17. R. Bekenstein, J. Nemirovsky, I. Kaminer, and M. Segev, "Shape-Preserving Accelerating Electromagnetic Wave Packets in Curved Space," Phys. Rev. X **4**(1), 011038 (2014).
18. B. O'neill, *Elementary Differential Geometry*, 2nd ed. (Academic Press, 2006).

#326390 https://doi.org/10.1364/OE.26.017820
Journal © 2018 Received 19 Mar 2018; revised 2 May 2018; accepted 5 May 2018; published 25 Jun 2018

Optics EXPRESS

1. Introduction

After Einstein described the gravitation with his general theory of relativity in 1915 [1], light propagation in curved space-time, which subverts common sense, attracts numerous research interests in both optics and astronomy physics [2–5]. In a curved space, the concept of straight line is generalized to be geodesic which corresponds to the shortest route between two points in a non-Euclidean geometry. By virtue of the absence of acceleration, geodesic curve accounts for the trajectory of free particle movement in curved space, which can be determined by the geodesic equation. From a physical point of view, this can be better interpreted as the conservation of momentum under the Clairaut parametrizations.

Interesting phenomena arising from curved space time have triggered the search for analogs of general relativity in many research fields [6–9]. For electromagnetic waves, inhomogeneous refractive index distribution mimics the effect of space-time curvature or gravitational potential. Recently novel concepts such as optical analog of black hole and celestial phenomena have been proposed and studied [10–14]. An alternative way for achieving curved space for light is by restricting the wave propagation onto a curved surface [15,16]. In all these cases, the wave is guided by the geodesic unless there is presence of acceleration that leads to non-geodesic route [17].

Here we study the light propagation on the surface of a torus, which is a two-dimensional curved closed manifold, whose topology, as described by the Gauss-Bonnet theorem, is a topological invariant given by the integral of Gaussian curvature. Based on the non-Euclidean geometry [18], geodesic curve as isometric invariant exists on the intrinsic surface of a torus, which can be explained by the conservation of the angular momentum of light around the direction of toroidal latitude circle as implied by the Noether's theorem. Compared to the previous work for a specialized problem on the influence of curvature on Gaussian beam propagating along the outer equator of torus [15], we here investigated the general case on the wave that originates from any point on the toroidal surface and propagates along any direction with a calculation method based on the conservation of the angular momentum. According to the propagation dynamics, waves on torus are classified into two categories: one that twists around the torus and sweeps across the whole surface area; the other one that is confined within certain latitude range of the torus, exhibits an interesting self-focusing or imaging behavior. The focusing point appears as an angular node around the torus, with the angular focusing length controlled by the geometric parameters of the torus and the latitude position of the light source.

2. Theory and simulations

Considering a point source S located on the toroidal surface as shown in Fig. 1(a), suppose that surface waves can be excited, for instance, within a thin film working as a waveguide coated on a toroidal perfect electric conductor, and will propagate on the toroidal surface towards all directions. The orbit angular momentum of the generated surface wave about the z-axis is conserved due to the rotation symmetry around the z-axis, which is given by:

$$\boldsymbol{L} = R_s \sin\alpha_s K_0 \hat{\boldsymbol{z}}, \tag{1}$$

where K_0 is the wave vector of the surface wave, R_s is the radius projection of source on the plane perpendicular to the z axis and $0 \le \alpha_s \le 2\pi$ denotes the direction of wave propagation as shown in Fig. 1(a). As a result of the conservation of L, the wave reaches a minimum radius R_c for a certain propagation direction which can be estimated as $R_c = R_s \sin\alpha_s$, where the sinusoidal value reaches the maximum. For a torus with outer and inner equator radii of R_1 and R_2 respectively, if $R_c < R_2$ the wave experiences no reflection and consequently can twist around the torus freely; on the other hand, if $R_c > R_2$, the wave is confined within the critical position of $R_c = R_2$ in a similar way as a total internal reflection process inside a graded index medium. By utilizing the transformation optics method as described in the Appendix, we

Optics EXPRESS

calculate the effective constitution parameters for Maxwell equations of the 2D torus in Euclidean space, and further confirm the two kinds of wave behaviors with wave simulation as shown in Figs. 1(b) and 1(c). For a point source on a torus with fixed geometry, the radiated surface waves propagate towards all possible directions, among which those with small value of $\alpha_s<\sin^{-1}(R_2/R_s)$ travel freely sweeping across the whole latitude range, while the others with larger peripheral angular momentum is bent back and restrained into trajectories within a limited latitude range on the torus. Interestingly, for the confined waves, they tend to be focused after travelling a certain distance as shown in Fig. 2(a), which presents the idea of surface wave focusing or imaging on the torus.

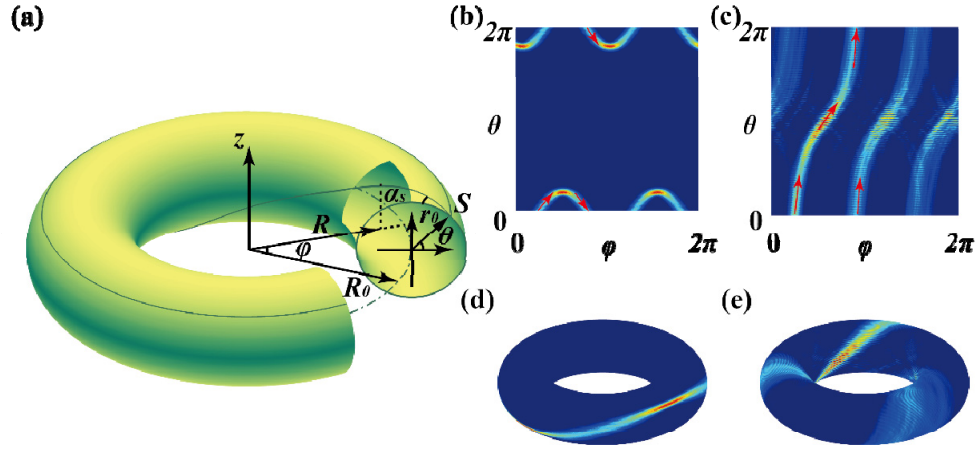

Fig. 1. (a) Schematic of torus coordinates with usual parametrization. The energy density of (b) reflected wave on a 2D torus. (c) free wave on 2D torus. (d) reflected wave on 3D space torus. (e) free wave on 3D space torus. The geometric parameters used in calculating the effective permittivity and permeability are R_1 = 3 m and R_2 = 3/2 m, the corresponding frequency is 10GHz.

When placing a point source on the outer equator of torus, as shown in Fig. 2(a), the propagation directions of paraxial waves are indicated as $\alpha_{\pm} = \pi/2 \pm \delta/2$, where $\delta/2$ is the angular deviation from the outer equator circle. The wave trajectory can be traced on the torus by the angular momentum conservation as per Eq. (1), showing that they meet each other after passing a longitudinal angle of φ_f as described in Fig. 2(a). We define φ_f as the angular focusing length, whose relationship with wave propagation direction α is shown in Fig. 2(b). One can see that φ_f is nearly constant for a certain range of α around $\alpha = \pi/2, 3\pi/2$. In contrast, when δ takes a larger value, the angular focusing length φ_f suffers from strong divergence, indicating that the waves with a large initial δ contribute very little to the focusing or imaging. As for the waves with initial directions α outside of the confined range, they twist around the torus and tend to diverge evenly over the surface.

We further consider the influence of geometric parameters on the imaging behavior. Under the paraxial approximation of the outer equator, we can calculate the relationship between the angular focusing length and the geometric parameters of torus to be

$$\varphi_f = \pi\sqrt{\frac{1}{2}-\frac{R_2}{2R_1}}, \tag{2}$$

where R_1 and R_2 as indicated in Fig. 2(a) are related to the equator radii shown in Fig. 1 as $R_0 = (R_1 + R_2)/2$ and $r_0 = (R_1-R_2)/2$. Since the equation does not show any frequency dependence, one expects that the angular focusing length φ_f is only determined by the geometry of the

Optics EXPRESS

torus, and thus the imaging process suffers no chromatic aberration which is a unique advantage of the geodesic systems. Figure 2(c) shows the dependence of the angular focusing length φ_f over the value of R_2/R_1. By choosing three different points on the φ_f vs R_2/R_1 curve, the corresponding φ_f-α dependence are calculated and plotted with different colors in Fig. 2(b). The φ_f-α curves strongly depend on the geometry. For a smaller value of R_2/R_1, a boarder flat region around $\alpha = \pi/2$ and $3\pi/2$ is achieved, implying that a broader range of waves can converge to the focusing point and hence a better imaging performance. In Figs. 2(d)-2(f), we employ the ray tracing method by neglecting the wave diffraction for calculating the field distribution, with the geometry parameters indicated in Fig. 2(c). The results confirm the different angular focusing lengths as $2\pi/3$, $\pi/2$ and $\pi/3$ for different parameters of torus, respectively. Moreover, when $R_2/R_1 \to -1$, the torus approaches a sphere and the image exactly appears at the opposite point of the source on the sphere, which gives the largest focusing length $\varphi_f = \pi$ when the source is located on the outer equator. When $R_2/R_1 \to 1$, most of waves diverge as expected, while the bounded waves get bent back quickly due to the extremely large curvature of torus along the meridian direction, leading to a diminishing focusing length.

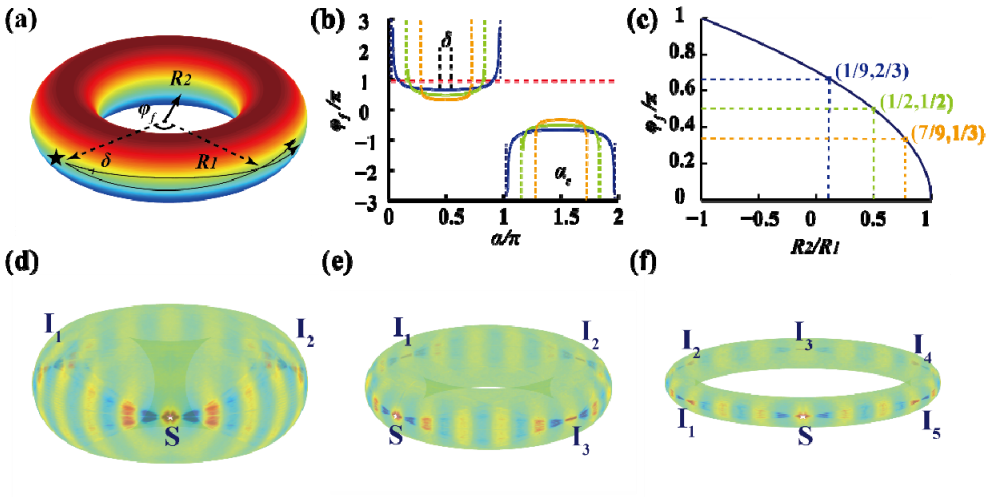

Fig. 2. (a) Schematic of light paraxial propagation around the outer radius. (b) The angular focusing length φ_f dependence on initial propagation angle α_s with different geometric parameters of torus. (c) Geometric parameters versus focusing length φ_f, where general points on curve will not guarantee integer number of focusing points within a single circle, several special points are marked and should correspond to closed geodesics. (d-f) Field distributions on torus with geometric parameters R_2 / R_1 = 1/9, 1/2 and 7/9, respectively. The wavelength is set as $\lambda = \pi R_1/10$ in the calculation.

We now focus on the closed light trajectories or geodesic curves on the torus, which correspond to the resonance of a propagation mode. For the confined rays, the angular focusing length in Eq. (2) can be used to determine the maximum number of bouncing for a closed geodesic curve within a single round trip along the torus meridian direction. From the equation we can see that the geodesic is closed when $2\sqrt{2/(1-R_2/R_1)}$ takes integer values. In the cases of R_2/R_1 = 1/9, 1/2 and 7/9 shown in Figs. 2(d)-2(f), the number of focusing nodes are integers of 3, 4 and 6, corresponding to the focusing lengths $\varphi_f = 2\pi/3$, $\pi/2$ and $\pi/3$, respectively. We verify the focusing nodes on the 2D torus by using wave simulation method as shown in Fig. 3. We can see that these focus nodes resulting from the closed light trajectory remain highly robust.

Optics EXPRESS

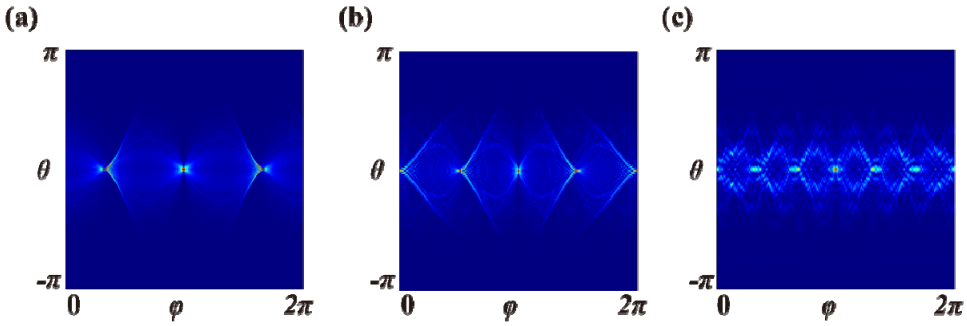

Fig. 3. Different number of focusing nodes for geometry parameters of R_2/R_1 = 1/9, 1/2 and 7/9 for (a-c) respectively, the field patterns are calculated with Comsol Multiphysics after using transformation optics method stated in the Appendix, the geometric parameters used in calculating the effective permittivity and permeability are R_2 = 1/3, 3/2, 7/3 m and R_1 = 3 m, the corresponding frequency is 10GHz.

Next, we study the wave propagation with a point source positioned slightly away from the outer equator. Again, we calculate the light trajectory by using the ray tracing method with a geometric parameter of R_2/R_1 = 1/2. As shown in Fig. 4(a), the neighboring images of the source are shifted away from the equator along opposite directions. A number of cases are studied with point source located at θ_s = 0, π/4, π/2 and 3π/4, as shown in Figs. 4(c)-4(f), respectively. From the field distributions, one can see that the images become blurred when the source is shifted away from the outer equator. This can be understood with the assistance of Fig. 4(b), where the φ_f-α curves are plotted. As can be seen, when the source is shifted away from the outer equator, the angular range within which the beams are confined becomes narrower. This means that a larger proportion of light will contribute to the background field distribution and the focus becomes boarder, which together lead to the blurring of the image. Meanwhile, it is worth noting that, when the position of the point source is changed, the angular focusing length is shifted, indicating that the focusing length can also be controlled by the location of point source in addition to the geometric parameters of torus, nevertheless at the expense of the imaging quality. An extreme case is when the point source is located on the inner equator, and all waves are free to travel on the torus and no focusing point can be found.

Optics EXPRESS

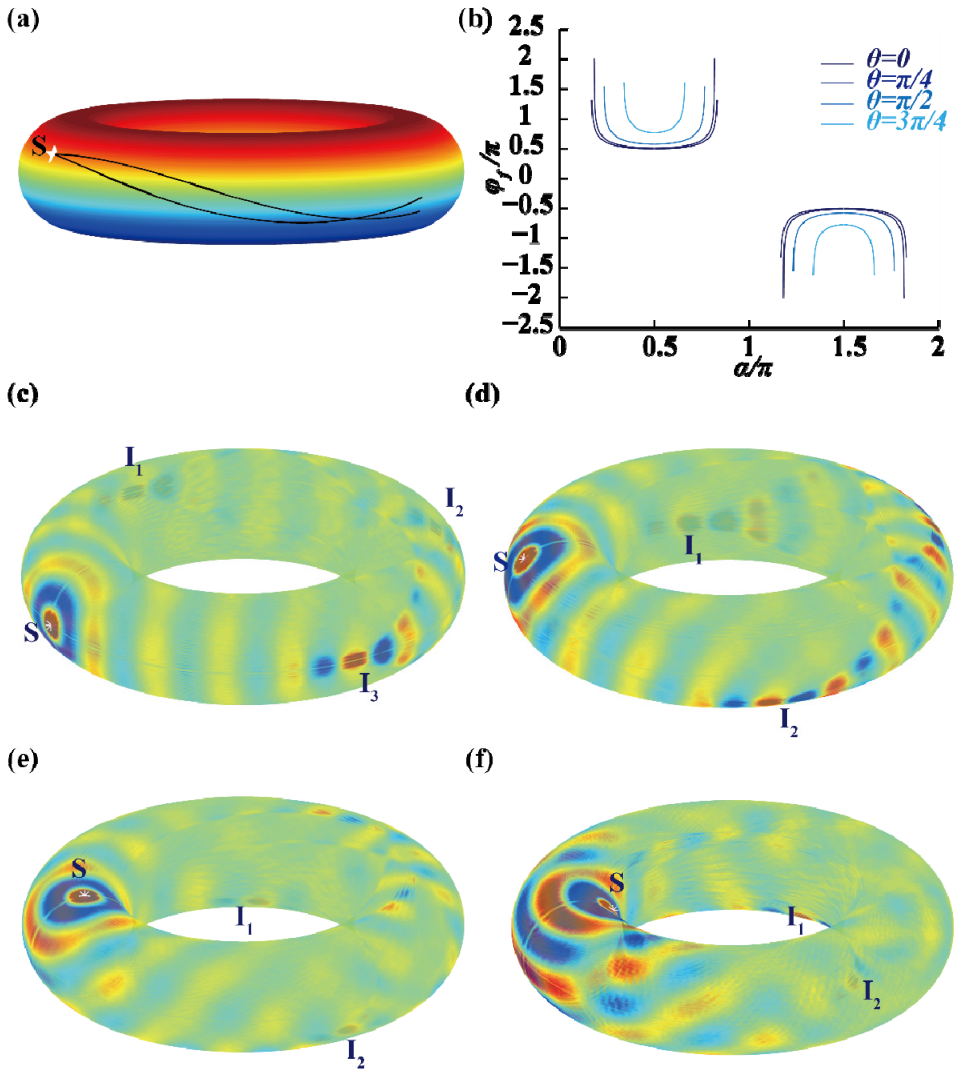

Fig. 4. (a) Schematic of light trajectory with an abaxial point source. (b) The φ_1-α relation for the point source located at different position. (c-f) Field distributions with different position of point source. The wavelength is set as $\lambda = \pi R_1/10$ in the calculation.

3. Conclusion

In conclusion, we have studied the wave propagation on the surface of a torus, which is a vivid example of light behavior on curved surface of manifolds with interesting topologies. On the torus surface, the angular momentum conservation law governs the behavior of wave propagation. Depending on the angle formed between the light ray and the outer equator, it can either twist around the torus or get bent back and stay confined to the outer brim of the torus. Focusing or imaging phenomenon with no chromatic aberration can be observed for paraxial beams. The angular focusing length can be controlled by either changing the geometry parameters of torus or choosing different source locations. Wave propagation on a torus surface opens doors to novel wave dynamic phenomena on the surface topological objects. Compared to conventional photonic structures are fabricated in planar settings, the

Optics EXPRESS

evolution of light can be controlled through the space curvature of the homogenous medium instead of the spatial variation of refractive index, providing a new 3D platform in integrated photonic circuits with Si or III-V semiconductors.

Appendix

1. Transformation optics method for effective constitution parameters.

For a torus with parametrization as

$$x = \left(R_0 + r_0\cos(\theta)\right)\cos(\phi)$$
$$y = \left(R_0 + r_0\cos(\theta)\right)\sin(\phi)$$
$$z = r_0\sin(\theta)$$

We consider a fixed shape ratio between two radii parameters as $r_0 = a \cdot R_0$, Then we can calculate the metric tensor to be [16,18]:

$$g_M = \begin{bmatrix} \frac{\partial}{\partial\phi}\cdot\frac{\partial}{\partial\phi} & \frac{\partial}{\partial\phi}\cdot\frac{\partial}{\partial\theta} & \frac{\partial}{\partial\phi}\cdot\frac{\partial}{\partial R_0} \\ \frac{\partial}{\partial\theta}\cdot\frac{\partial}{\partial\phi} & \frac{\partial}{\partial\theta}\cdot\frac{\partial}{\partial\theta} & \frac{\partial}{\partial\theta}\cdot\frac{\partial}{\partial R_0} \\ \frac{\partial}{\partial R_0}\cdot\frac{\partial}{\partial\phi} & \frac{\partial}{\partial R_0}\cdot\frac{\partial}{\partial\theta} & \frac{\partial}{\partial R_0}\cdot\frac{\partial}{\partial R_0} \end{bmatrix} \begin{bmatrix} x \\ y \\ z \end{bmatrix} = \begin{bmatrix} g_{\phi\phi} & g_{\phi\theta} & g_{\phi R_0} \\ g_{\theta\phi} & g_{\theta\theta} & g_{\theta R_0} \\ g_{R_0\phi} & g_{R_0\theta} & g_{R_0R_0} \end{bmatrix}$$

with the metric tensor components written as,

$$g_{\phi\phi} = \left(R_0 + aR_0\cos(\theta)\right)^2\left(4e^2\sin^2(2\phi)+1\right)$$
$$g_{\phi\theta} = g_{\theta\phi} = 0$$
$$g_{\phi R_0} = g_{R_0\phi} = 0$$
$$g_{\theta\theta} = a^2R_0^2$$
$$g_{\theta R_0} = g_{R_0\theta} = -aR_0\sin(\theta)\left(1+a\cos(\theta)\right) + a^2R_0\cos(\theta)\sin(\theta)$$
$$g_{R_0R_0} = 1 + a^2 + 2a\cos(\theta)$$

For a general space with no source, the Maxwell equations can be written as [14],

$$\left(\sqrt{g}g^{ij}E_j\right)_{,i} = 0$$
$$\left(\sqrt{g}g^{ij}B_j\right)_{,i} = 0$$
$$[ijk]E_{k,j} = -\frac{\partial\left(\pm\sqrt{g}g^{ij}B_j\right)}{\partial t}$$
$$[ijk]B_{k,j} = -\frac{1}{c^2}\frac{\partial\left(\pm\sqrt{g}g^{ij}E_j\right)}{\partial t}$$

where g is the determinant of matrix g_M, according to the equivalence of Maxwell equations in empty curved space and in Euclidean space with medium, the geometric parameters can be transformed as the effective constitution parameters for 2D torus in Euclidean space, can be calculated as

Optics EXPRESS

$$\varepsilon = \mu = \pm\sqrt{g}\,g_M^T$$

and superscript stands for transpose.

2. Derivation of the angular focusing length equation

For the toroidal surface, we have the following relationships [18]

$$ds^2 = R_0^2\cos^2\theta d\varphi^2 + r_0^2 d\theta^2 \tag{1}$$

$$d\varphi = \frac{\sin\alpha}{R}ds \tag{2}$$

$$d\theta = \frac{\cos\alpha}{r_0}ds \tag{3}$$

Then we can have

$$d\varphi = \frac{r_0}{R}\tan\alpha d\theta \tag{4}$$

Consider the orbital angular momentum at the source position,

$$L_s = R_s\sin\alpha_s k_0 \tag{5}$$

And at arbitrary position along the light trajectory,

$$L = R\sin\alpha k_0 \tag{6}$$

Due to the conversion of orbit angular momentum, combine [5] and [6], we can get

$$R = \frac{R_s\sin\alpha_s}{\sin\alpha} \tag{7}$$

At the same time, from the parametrization we have

$$R = R_0 + r_0\cos\theta \tag{8}$$

Taking the derivative of both equations gives:

$$dR = -r_0\sin\theta d\theta = -\frac{\cos\alpha}{\sin^2\alpha}R_s\sin\alpha_s d\alpha \tag{9}$$

And following gives:

$$d\theta = \frac{R_s\sin\alpha_s\cos\alpha}{r_0\sin^2\alpha}\frac{1}{\sin\theta}d\alpha \tag{10}$$

Also from [7,8] we can have

$$\sin\theta = \sqrt{1-\left(\frac{R_s\sin\alpha_s}{r_0\sin\alpha} - \frac{R_0}{r_0}\right)^2} \tag{11}$$

Substitute [7,10,11] into [4] to give

Optics EXPRESS

$$d\varphi = \frac{1}{\sqrt{1-\left(\frac{R_s \sin\alpha_s}{r_0 \sin\alpha} - \frac{R_0}{r_0}\right)^2}} d\alpha \tag{12}$$

Then we can get the angular focusing length by taking the paraxial limitation of the integral,

$$\varphi_f = 2 \lim_{\alpha_s \to \frac{\pi}{2}} \int_{\alpha_s}^{\frac{\pi}{2}} \frac{1}{\sqrt{1-\left[\frac{(R_0 + r_0)\sin\alpha_s}{r_0 \sin\alpha} - \frac{R_0}{r_0}\right]^2}} d\alpha = \frac{\pi}{\sqrt{\frac{R_0 + r_0}{r_0}}} \tag{13}$$

3. Verification of non-achromatic feature

We take the transformation method to get the permittivity and permeability tensor and put them into wave simulation with commercial software COMSOL Multiphysics, and the simulation result are shown in Fig. 5.

Optics EXPRESS

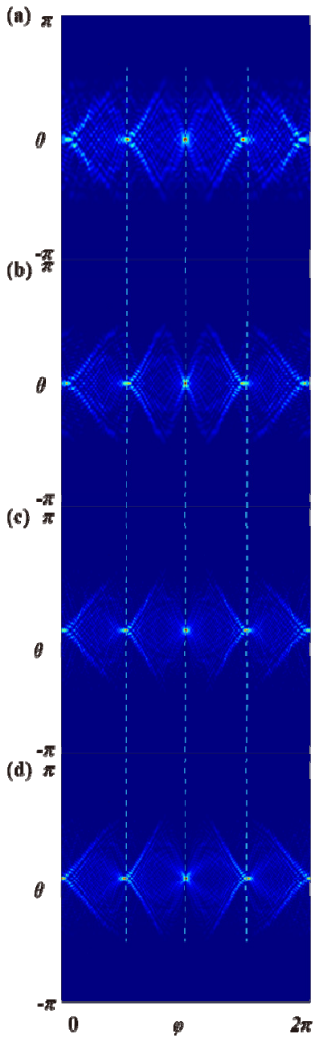

Fig. 5. Wave propagation in the 2D torus for different frequencies: 3 - 6 GHz for (a) - (d) respectively. The geometric parameters used in calculating the effective permittivity and permeability are $R_1 = 3$ m and $R_2 = 3/2$ m.

Funding

ERC Consolidator Grant (TOPOLOGICAL), the Royal Society and the Wolfson Foundation, the Leverhulme Trust (RPG-2012-674), and the Engineering and Physical Sciences Research Council (EP/J018473/1).